

# Observation of a Griffiths phase

**J. Deisenhofer<sup>1</sup>, D. Braak<sup>2</sup>, H.-A. Krug von Nidda<sup>1</sup>, J. Hemberger<sup>1</sup>, R.M. Eremina<sup>3</sup>, V.A. Ivanshin<sup>4</sup>, A.M. Balbashov<sup>5</sup>, A. Loidl<sup>1</sup>, T. Kimura<sup>6</sup> & Y. Tokura<sup>6</sup>**

<sup>1</sup>*EP V, Center for Electronic Correlations and Magnetism, University of Augsburg, 86135 Augsburg, Germany*

<sup>2</sup>*TP II, Institute for Physics, University of Augsburg, 86135 Augsburg, Germany*

<sup>3</sup>*E. K. Zavoisky Physical-Technical Institute, 420029 Kazan, Russia*

<sup>4</sup>*Kazan State University, 420008 Kazan, Russia*

<sup>5</sup>*Moscow Power Engineering Institute, 105835 Moscow, Russia*

<sup>6</sup>*Department of Applied Physics, University of Tokyo, Tokyo 113-8656, Japan*

**When Griffiths<sup>1</sup> explored the effects of random dilution on the magnetization of an Ising ferromagnet in 1969, science was enriched by a fundamental concept of randomness in systems undergoing an ordering transition. For example, the ordering of spins in ferromagnets<sup>2</sup> or the unbinding of biopolymers in DNA<sup>3</sup>. In solid-state physics Griffiths scenarios have been evoked to account for such challenging physical problems as the non-Fermi liquid behavior in Kondo systems<sup>4</sup>, the phenomenon of colossal magnetoresistance<sup>5</sup>, and the properties of magnetic semiconductors<sup>6</sup>. To date, however, an entire Griffiths phase had not been identified experimentally. Here we report the discovery of a Griffiths phase in the manganite system  $\text{La}_{1-x}\text{Sr}_x\text{MnO}_3$ . Using electron spin resonance and magnetic susceptibility measurements, we find a triangular phase regime that is limited by the percolation threshold  $x_c \sim 0.07$ , the Griffiths temperature  $T_G \approx 270$  K, and the ferromagnetic transition temperature up to the Sr concentration  $x_{\text{max}} \sim 0.16$ .**

Upon doping the superexchange (SE) coupled antiferromagnetic (AFM) insulator  $\text{LaMnO}_3$  with Ca/Sr the system proves to be a treasure chest for rich and puzzling physics<sup>7,8</sup>. For  $\text{La}_{1-x}\text{Sr}_x\text{MnO}_3$  the parameter space including spin, charge, lattice, and orbital degrees of freedom is particularly complex in the regime  $0 \leq x \leq 0.2$  (ref. 9,10), far below the regime where colossal magnetoresistance effects<sup>5,11</sup> are observed. With increasing  $x$  the number of  $\text{Mn}^{4+}$  ions rises and the probability of ferromagnetic (FM) bonds in the system is enhanced by double-exchange (DE) between  $\text{Mn}^{3+}$  and  $\text{Mn}^{4+}$  ions. On the background of a cooperatively JT distorted orthorhombic structure the ground state of  $\text{La}_{1-x}\text{Sr}_x\text{MnO}_3$  evolves with increasing  $x$  from an AFM insulator to a FM insulating (FMI) state and on to a FM metal<sup>12,13</sup> at  $x \sim 0.20$ . We provide experimental evidence that the complex parameter space of  $\text{La}_{1-x}\text{Sr}_x\text{MnO}_3$  exhibits a phase that remained both ubiquitous in literature<sup>14</sup> on solid-state physics and evasive of experimental identification since its prediction by Griffiths<sup>1</sup>.

Starting from an Ising type model - where the magnetic spin moments on a lattice site have only two possible orientations, either up or down - with FM bond strengths  $J$  between nearest-neighbor sites, Griffiths allowed for disorder in the magnetic system by associating the existence of a FM bond  $J$  with probability  $p \leq 1$  and, correspondingly, the absence of a bond with probability  $1-p$ . In such a diluted ferromagnet, the values of  $J$  are fixed within the lattice (quenched disorder) and assumed to be statistically independent. Their distribution is therefore given in terms of the fraction  $p$  of occupied bonds which naturally determines the magnetization  $M$  of the system. Figure 1a shows schematically the resulting  $T$ - $p$  phase diagram. Due to randomness the FM ordering temperature  $T_C(p)$  is always lower than that in the pure ( $p=1$ ) system  $T_C(p) < T_C(1)$  and reaches zero at the percolation threshold  $p_c$  of the bond distribution  $T_C(p_c)=0$ . For  $p \geq p_c$  there exists an infinite percolating cluster of FM bonds that accounts for  $T_C(p) > 0$ , while for  $p < p_c$  there are only finite connected regions and the system remains paramagnetic (PM) down to lowest temperatures. Griffiths argued that the magnetization  $M(T, H)$  is

nonanalytic as a function of magnetic field  $H$ , i.e. it has a singularity at  $H=0$ , at temperatures  $T_C(p) < T < T_G$  due to the presence of premagnetized regions within the globally PM system. This singularity is usually considered to be weak (an exception is the one-dimensional model studied by McCoy<sup>15</sup>) and the quest for Griffiths' phase concentrated on dynamic measurements such as slow relaxation of the magnetization<sup>2,4,6</sup>. However, the predicted features like stretched exponential behaviour turn out to be very common among a variety of materials<sup>16</sup> and, hence, their significance as a crucial tool to reveal Griffiths phase boundaries is obviously limited. Griffiths derived a lower bound for the temperature  $T_G$ , namely the ordering temperature of the pure system  $T_G=T_C(1)$  which is independent of  $p$ . As seen in the schematic phase diagram in Fig. 1a, the phase boundaries  $p_c$ ,  $T_C(p)$ , and  $T_G$  define a percolative Griffiths-phase triangle (GPT). We will identify these phase boundaries in  $\text{La}_{1-x}\text{Sr}_x\text{MnO}_3$  and show that a theoretical construct like the GPT occurs in real systems.

Using electron spin resonance (ESR) one can, in general, investigate the local environment and the spin dynamics of PM ions<sup>17</sup> and the oscillations of the magnetization in magnetically ordered systems<sup>18</sup>. In Fig. 2 we show the ESR spectra in  $\text{La}_{0.875}\text{Sr}_{0.125}\text{MnO}_3$  in the PM regime above magnetic ordering. The spectra consist of a PM signal due to the majority of  $\text{Mn}^{3+}$  and  $\text{Mn}^{4+}$  spins<sup>19</sup> and of a weak but decisive FM resonance (FMR) signal at lower resonance fields. An expansion of the temperature dependence of the FMR is shown in Fig. 3 as a 2D-contour plot. At  $T \gtrapprox 260$  K, far above magnetic ordering at  $T_C=180$  K (see ref. 13), the FMR emerges from the signal of the PM  $\text{Mn}^{3+}/\text{Mn}^{4+}$  background at  $g=2$  and shifts towards lower resonance fields indicating the increase of local magnetic fields in the sample. This shift corresponds to the temperature dependence of the FM magnetization<sup>18</sup>. Concomitantly, the intensity of the FMR first clearly increases and then saturates with decreasing temperatures excluding a PM or superparamagnetic origin of the signal, which would result in a Curie-Weiss (CW) like increase instead of saturation. As shown in the upper inset of Fig. 2, the PM

line broadens, shifts to lower resonance fields on approaching  $T_C$  (similar to the appearance of the FMR), and finally merges with the FMR (see also Fig. 4(b)). The FMR signal exhibits a pronounced easy-plane anisotropy (in the plane of FM superexchange coupling) yielding an anisotropy field of about 2.7 kOe in agreement with the value found by neutron scattering<sup>20</sup> confirming the intrinsic origin of the FMR. These FMR signals were observed in the PM regime above  $T_C$  in single crystals with Sr concentrations  $x = 0.075, 0.1, 0.125, 0.15$ . They all separate from the PM signal below 270 K indicating a temperature scale above  $T_C$  which is independent of  $x$ . We want to point out that for  $x \leq 0.05$  no FMR was observed in the PM regime suggesting the existence of a lower Sr concentration threshold  $x_c$  with  $0.05 < x_c < 0.075$ . From the ESR spectra one can deduce that the net magnetization responsible for the FMR is about three orders of magnitude less than the PM magnetization, i.e. the majority of the spins is still in the PM state. In Fig. 4a we show susceptibility data for  $\text{La}_{0.9}\text{Sr}_{0.1}\text{MnO}_3$  together with the temperature dependence of the resonance fields of both the FMR and the PM signal (Fig. 4b). For a large applied magnetic field (1 kOe) the FM component is hidden in the PM contribution and a CW law is found throughout the PM regime, while in small magnetic fields (10 Oe) clear deviations from a CW behaviour are observed below  $T_G \approx 270$  K (Fig. 4a). This temperature agrees very well with the extrapolation of the FMR shift with respect to  $g=2$  using a standard saturation behaviour  $\sim (1-T/T_G)^{1/2}$  (Fig. 4b). The obtained temperatures  $T_G(x)$  are plotted within the established phase diagram<sup>13</sup> of  $\text{La}_{1-x}\text{Sr}_x\text{MnO}_3$  in Fig. 1b. We find a Griffiths temperature  $T_G \sim 270$  K that is nearly independent of  $x$ , identifying the upper phase boundary of the GPT. Within the GPT ( $T_C < T < T_G$ ) the percolating cluster of FM bonds becomes premagnetized building up FM domains. The resulting small net magnetization is evidenced by the FMR signal in the ESR spectra. Naturally, the FM ordering temperatures constitute the lower phase boundary of the GPT. At  $T_C$  the premagnetized domains of the percolating cluster align spontaneously, giving rise to a slight decrease of the resistivity<sup>13</sup>.

After identification of the temperature boundaries of the GPT, let us now explore the realization of the percolation threshold  $p_c$  and the case corresponding to  $p=1$ : The probability  $p$  of a FM bond is associated with the Sr concentration  $x$  in our system, which arises from an enhanced FM exchange interaction with increasing number of  $Mn^{4+}$  ions in the system. From the intersection of the  $T_G$  boundary with the magnetic ordering boundary (Fig. 1a), the FM regime corresponding to  $p=1$  is found to be at  $x \sim 0.16$ . In a generalization of Griffiths' concept to FM systems with an arbitrary distribution of bond strengths, the Griffiths temperature scale  $T_G$  is no longer the critical temperature of the pure FM system with  $p=1$  but the maximal critical temperature among all configurations compatible with the static nature of disorder<sup>21</sup>. In our case, the static disorder is annealed at  $x_{max} \sim 0.16$  as a consequence of the transition from the JT distorted orthorhombic to the rhombohedral phase, i.e. as the random locations of the FM bonds begin to fluctuate concomitantly with the fluctuating lattice distortions. Consequently, the Griffiths phenomenon disappears for  $x > 0.16$ . The threshold regime  $0.05 < x_c < 0.075$  derived from the existence of the FMR in our ESR spectra can be refined by taking into account the results of neutron-diffraction studies<sup>22</sup> in a single crystal with  $x=0.07$ . At this concentration the system is mainly in the canted AFM state, but an estimated 10 % of the crystal volume is in a FM state. Such a coexistence at low temperatures is to be expected in the vicinity of the percolation threshold where singularities of a different nature may emerge<sup>23</sup>. In contrast, for  $x=0.06$  no such features were found<sup>24</sup> narrowing the percolation threshold regime to  $0.06 < x_c < 0.075$ . Considering DE only, a lower bound for the percolation threshold is 1/8 of the site percolation value 0.3116 for a simple cubic lattice<sup>25</sup> resulting in  $x_c > 0.04$  in agreement with our experimental range. As a consequence of the AFM bonds in the system, the ordering temperature does not vanish at  $x_c$  but canted AFM order appears for  $x < x_c$ . Indeed, Burgi *et al.*<sup>11</sup> argue on theoretical grounds that the existence of a competing phase (here AFM) stabilizes and enhances FM Griffiths-like effects occurring below a temperature  $T^* > T_C$ .

In combination with the strong quenching of the disorder by the JT effect, this may offer the explanation for the appearance of a Griffiths phase in manganites and the observability by ESR, while its features remained hidden in many other FM materials.

In summary, a triangular Griffiths phase regime has been identified in the  $T$ - $x$  phase diagram of  $\text{La}_{1-x}\text{Sr}_x\text{MnO}_3$  by means of ESR and susceptibility measurements. The importance of quenched disorder<sup>11,26,27</sup> for the occurrence of a Griffiths phase in manganites cannot easily be overestimated. The observed GPT crowns the FMI phase that has been puzzling researchers for more than a decade<sup>8,28</sup>. Conspiracy of nature or general concept, this remarkable coincidence seems to also appear in the similar system  $\text{La}_{1-x}\text{Ca}_x\text{MnO}_3$ , where the persistence of a FMR has been observed above magnetic ordering in the concentration regime of the FMI ground state<sup>29</sup>. We propose, therefore, that analogously to our observation a Griffiths phase triangle should also crown the FMI dome in  $\text{La}_{1-x}\text{Ca}_x\text{MnO}_3$  with a percolation threshold  $x_c \sim 0.08$  and  $x_{\max} \sim 0.22$  (ref. 30).

## Methods

Single crystals of  $\text{La}_{1-x}\text{Sr}_x\text{MnO}_3$  were grown by the floating zone method. ESR measurements were performed with a commercial CW spectrometer at X- (9.4 GHz) and Q-band frequencies (34 GHz), using a continuous gas-flow cryostat for He. The crystals were oriented using Laue X-ray diffraction and mounted on quartz tubes. A goniometer allowed the rotation of the sample around an axis perpendicular to the static magnetic field. ESR detects the power  $P$  absorbed by the sample from the transverse magnetic microwave field as a function of the static magnetic field  $H$ . The signal-to-noise ratio of the spectra is improved by recording the derivative  $dP/dH$  using lock-in technique with field modulation. In principle, the intensity of the absorption spectrum measures the spin susceptibility of the resonant spins and the resonance shift with respect to the free electron value  $g=2$  provides information on local magnetic fields at

the spins' site. The magnetic susceptibility was measured using a commercial superconducting quantum interference device (SQUID) magnetometer.

1. Griffiths, R. B., Nonanalytic behavior above the critical point in a random Ising ferromagnet. *Phys. Rev. Lett.* **23**, 17-19 (1969).
2. Bray, A. J., Nature of the Griffiths Phase. *Phys. Rev. Lett.* **59**, 586-589 (1987).
3. Kafri, Y., & Mukamel, D., Griffiths singularities in unbinding of strongly disordered polymers. *Phys. Rev. Lett.* **91**, 055502 (2003).
4. Castro Neto, A. H., Castilla, G., & Jones, B. A., Non-Fermi Liquid Behaviour and Griffiths Phase in *f*-Electron Compounds. *Phys. Rev. Lett.* **59**, 3531-3534 (1998).
5. Salamon, M. B., Lin, P., & Chun, S. H., Colossal Magnetoresistance is a Griffiths Singularity. *Phys. Rev. Lett.* **88**, 197203 (2002).
6. Galitski, V. M., Kaminski, A., & Das Sarma, S., Griffiths Phase in Diluted Magnetic Semiconductors. *Phys. Rev. Lett.* **92**, 177203 (2004).
7. De Teresa, J. M., *et al.*, Evidence for magnetic polarons in magnetoresistive perovskites. *Nature* **386**, 256-259 (1997).
8. Yamada, Y., *et al.*, Polaron Ordering in Low-Doping  $\text{La}_{1-x}\text{Sr}_x\text{MnO}_3$ . *Phys. Rev. Lett.* **77**, 904-907 (1996).
9. Tokura, Y., & Nagaosa, N., Orbital Physics in Transition Metal Oxides. *Science* **288**, 462-468 (2000).
10. Dagotto, E., Hotta, T., & Moreo, A., Colossal magnetoresistant materials: the key role of phase separation. *Phys. Rep.* **344**, 1-153 (2001).

11. Burgy, J., Mayr, M., Martin-Mayor, V., Moreo, A., & Dagotto, E., Colossal Effects in Transition Metal Oxides Caused by Intrinsic Inhomogeneities. *Phys. Rev. Lett.* **87**, 277202 (2001).
12. Kawano, H., Kajimoto, R., Kubota, M., & Yoshizawa, H., Canted antiferromagnetism in an insulating lightly doped  $\text{La}_{1-x}\text{Sr}_x\text{MnO}_3$  with  $x \leq 0.17$ . *Phys. Rev. B* **53**, 2202-2205 (1996).
13. Paraskevopoulos, M., *et al.*, Magnetic properties and the phase diagram of  $\text{La}_{1-x}\text{Sr}_x\text{MnO}_3$  for  $x \leq 0.2$ . *J. Phys.: Condens. Matter* **12**, 3993-4011 (2000).
14. Green, C., & Lebowitz, J.L., *Phase Transitions and Critical Phenomena*. Vol. 7 (Academic Press, London, 1983).
15. McCoy, B.M., Theory of a two-dimensional Ising Model with Random Impurities III. Boundary Effects. *Phys. Rev.* **188**, 1014 (1969).
16. Palmer, R.G., Stein, D.L., Abrahams, E., & Anderson, P.W., Models of Hierarchically Constrained Dynamics for Glassy Relaxation. *Phys. Rev. Lett.* **53**, 958-961 (1984).
17. Abragam, A., & Bleaney, B., *Electron Paramagnetic Resonance of Transition Ions* (Clarendon, Oxford, 1970).
18. Gurevich, A.G., & Melkov, G.A., *Magnetization Oscillations and Waves* (CRC Press, Boca Raton, 1996).
19. Ivanshin, V.A., *et al.*, ESR study in lightly doped  $\text{La}_{1-x}\text{Sr}_x\text{MnO}_3$ . *Phys. Rev. B* **61**, 6213-6219 (2000).
20. Vasiliu-Doloc, L., Lynn, J.W., Moudden, A.H., de Leon-Guevara, A.M., & Revcolevschi, A., Structure and spin dynamics of  $\text{La}_{0.85}\text{Sr}_{0.15}\text{MnO}_3$ . *Phys. Rev. B* **58**, 14913-14921 (1998).

21. Bray, A.J., & Moore, M.A., On the eigenvalue spectrum of the susceptibility matrix for random spin systems. *J. Phys. C: Solid State Phys.* **15**, L765-L771 (1982).
22. Dubunin, S.F., *et al.*, Phase Separation of the Spin System in the  $\text{La}_{0.93}\text{Sr}_{0.07}\text{MnO}_3$  Crystal. *Phys. Solid State* **45**, 2297-2302 (2003).
23. Bakri, M. M., & Stauffer, D., Essential singularities in dilute magnets. *Phys. Rev. B* **14**, 4215-4218 (1976).
24. Hennion, M., *et al.*, Evidence of anisotropic magnetic polarons in  $\text{La}_{0.94}\text{Sr}_{0.06}\text{MnO}_3$  by neutron scattering and comparison with Ca-doped manganites. *Phys. Rev. B* **61**, 9513-9522 (2000).
25. Stauffer, D., & Aharony, A., *Introduction to Percolation Theory* (Taylor & Francis, London, 1992).
26. Nakajima, T., Yoshizawa, H., & Ueda, Y., A-site Randomness Effect on Structural and Physical Properties of Ba-based Perovskite Manganites. *J. Phys. Soc. Jpn.* **73**, 2283-2291 (2004).
27. Tomioka, Y., & Tokura, Y., Global phase diagram of perovskite manganites in the plane of quenched disorder versus one-electron bandwidth. *Phys. Rev. B* **70**, 014432 (2004).
28. Endoh, Y., *et al.*, Transition between Two Ferromagnetic States Driven by Orbital Ordering in  $\text{La}_{0.88}\text{Sr}_{0.12}\text{MnO}_3$ . *Phys. Rev. B* **82**, 4328-4331 (1999).
29. Markovich, V., *et al.*, Magnetic, transport, and electron magnetic resonance properties of  $\text{La}_{0.82}\text{Ca}_{0.18}\text{MnO}_3$  single crystals. *Phys. Rev. B* **65**, 144402 (2002).
30. Okuda, T., Tomioka, Y., Asamitsu, A., and Tokura, Y., Low-temperature properties of  $\text{La}_{1-x}\text{Ca}_x\text{MnO}_3$  single crystals: Comparison with  $\text{La}_{1-x}\text{Sr}_x\text{MnO}_3$ . *Phys. Rev. B* **61**, 8009-8015 (2000).

Acknowledgments We thank M.V. Eremin, K.-H. Höck, G. Jug, T. Kopp, L. Svistov, and K. Ziegler for fruitful discussions. This work was supported by BMBF/EKM and by DFG/SFB Augsburg.

Competing interests statement The authors declare that they have no competing financial interests.

Correspondence and requests for materials should be addressed to J.D. (email: [joachim.deisenhofer@physik.uni-augsburg.de](mailto:joachim.deisenhofer@physik.uni-augsburg.de)).

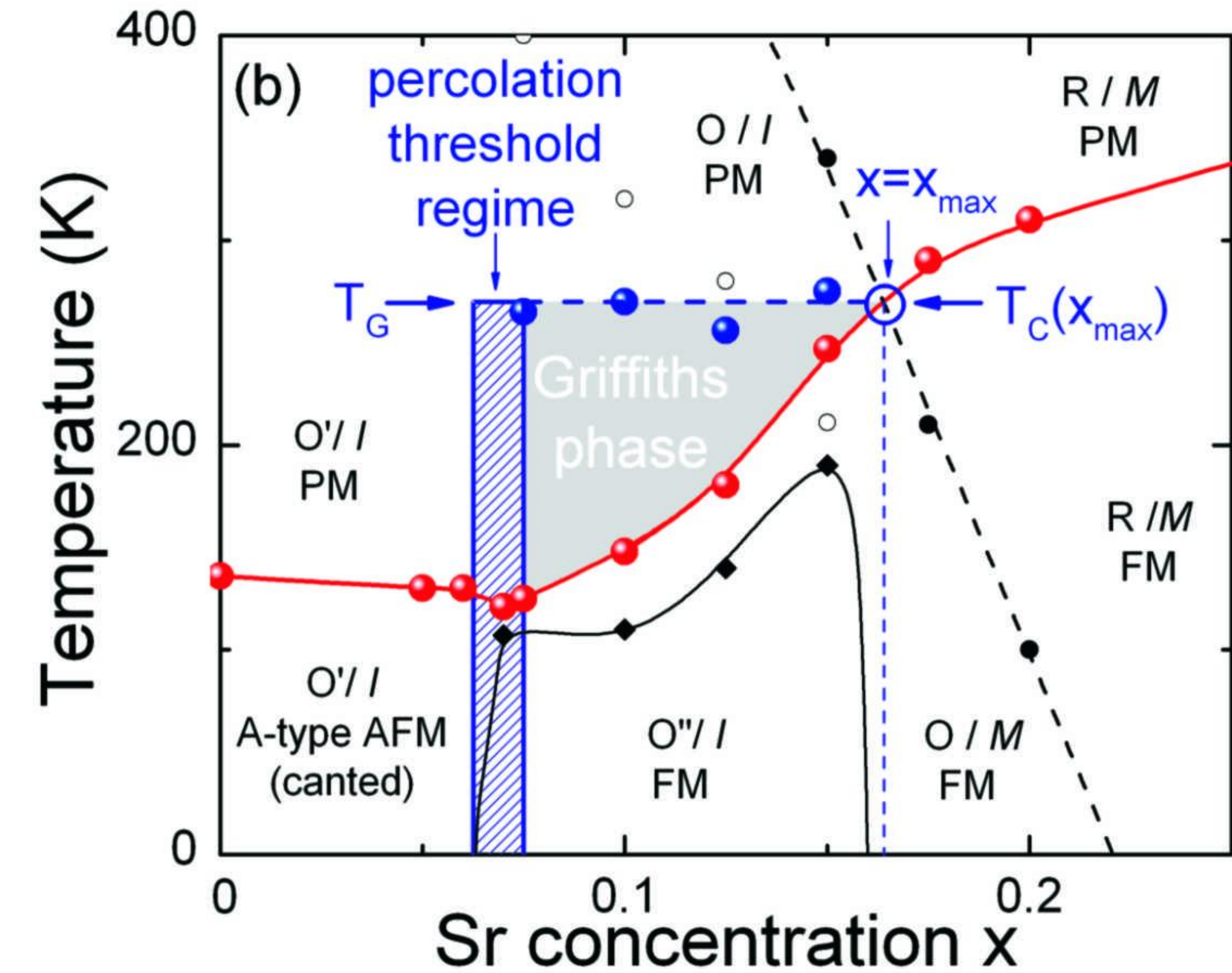
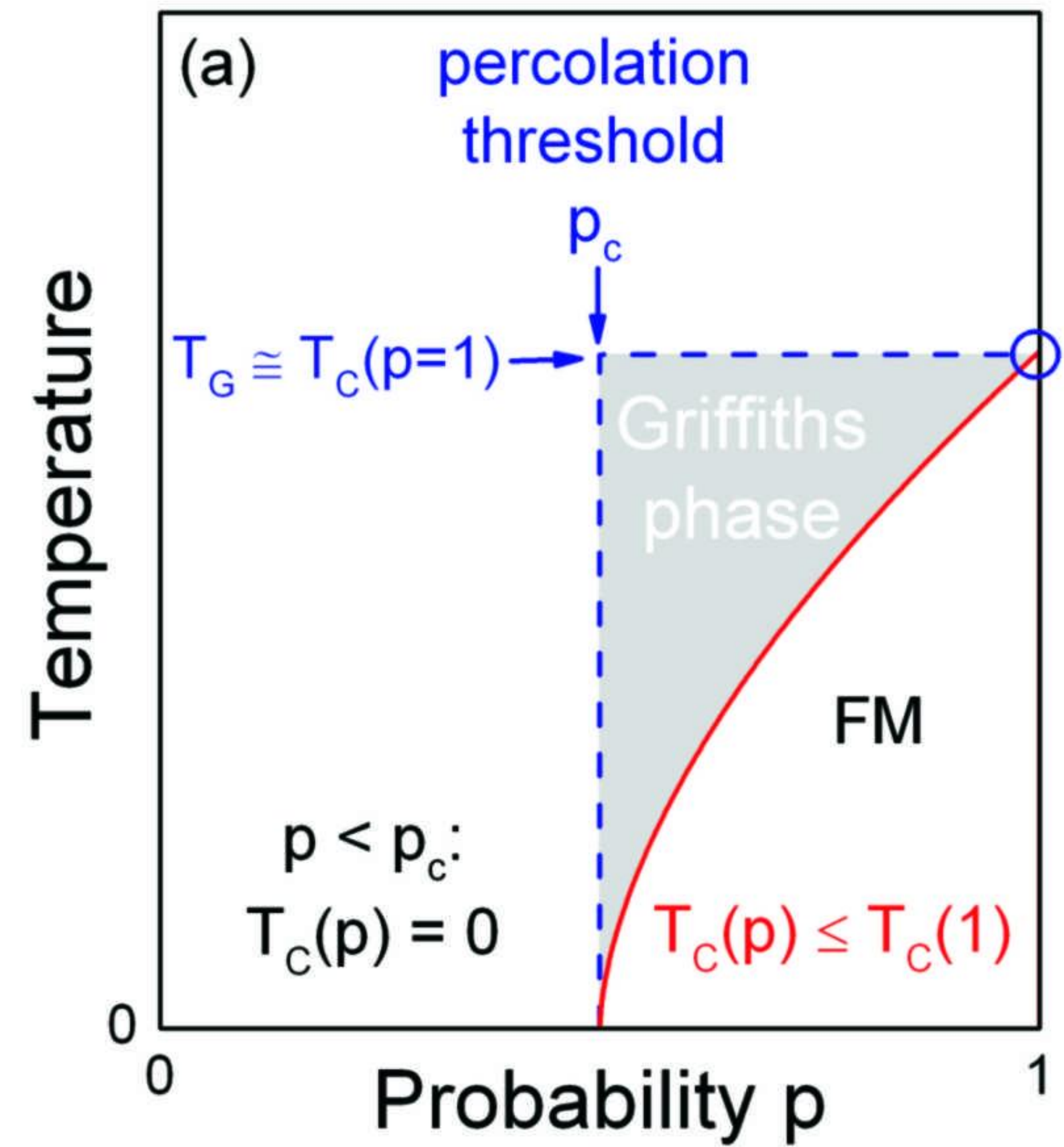
**Figure 1** New triangular phase regime in the  $T$ - $x$  phase diagram of  $\text{La}_{1-x}\text{Sr}_x\text{MnO}_3$ . **a**, Schematic  $T$ - $p$  diagram defining the characteristic features of the Griffiths phase triangle, i.e. the  $p$ -independent Griffiths temperature  $T_G$ , the percolation threshold  $p_c$ , and the magnetic phase boundary given by  $T_C(p)$ . **b**,  $T$ - $x$  phase diagram of  $\text{La}_{1-x}\text{Sr}_x\text{MnO}_3$  (see ref. 13) identifying the GPT boundaries. The intersection (blue circle) of  $T_G$  (blue spheres) with the magnetic boundary  $T_C$  (red spheres) coincides with the phase transition from the orthorhombic (O) to rhombohedral (R) structure (I = insulator, M = metal). Open circles and solid diamonds indicate phase boundaries of different orthorhombic phases. Temperatures for  $x=0.06$  and 0.07 were taken from ref. 24 and 22, respectively. Lines are drawn to guide the eyes.

**Figure 2** ESR spectra in  $\text{La}_{0.875}\text{Sr}_{0.125}\text{MnO}_3$  for  $205 \text{ K} \leq T \leq 253 \text{ K}$ . The spectra consist of a PM signal at  $g=2$  and a FMR at lower resonance fields. The external magnetic field was applied within the easy plane. The FMR at 225 K is highlighted in the lower inset using the same color scale as in Fig. 3. The upper inset shows the evolution of the spectra towards  $T_C$ .

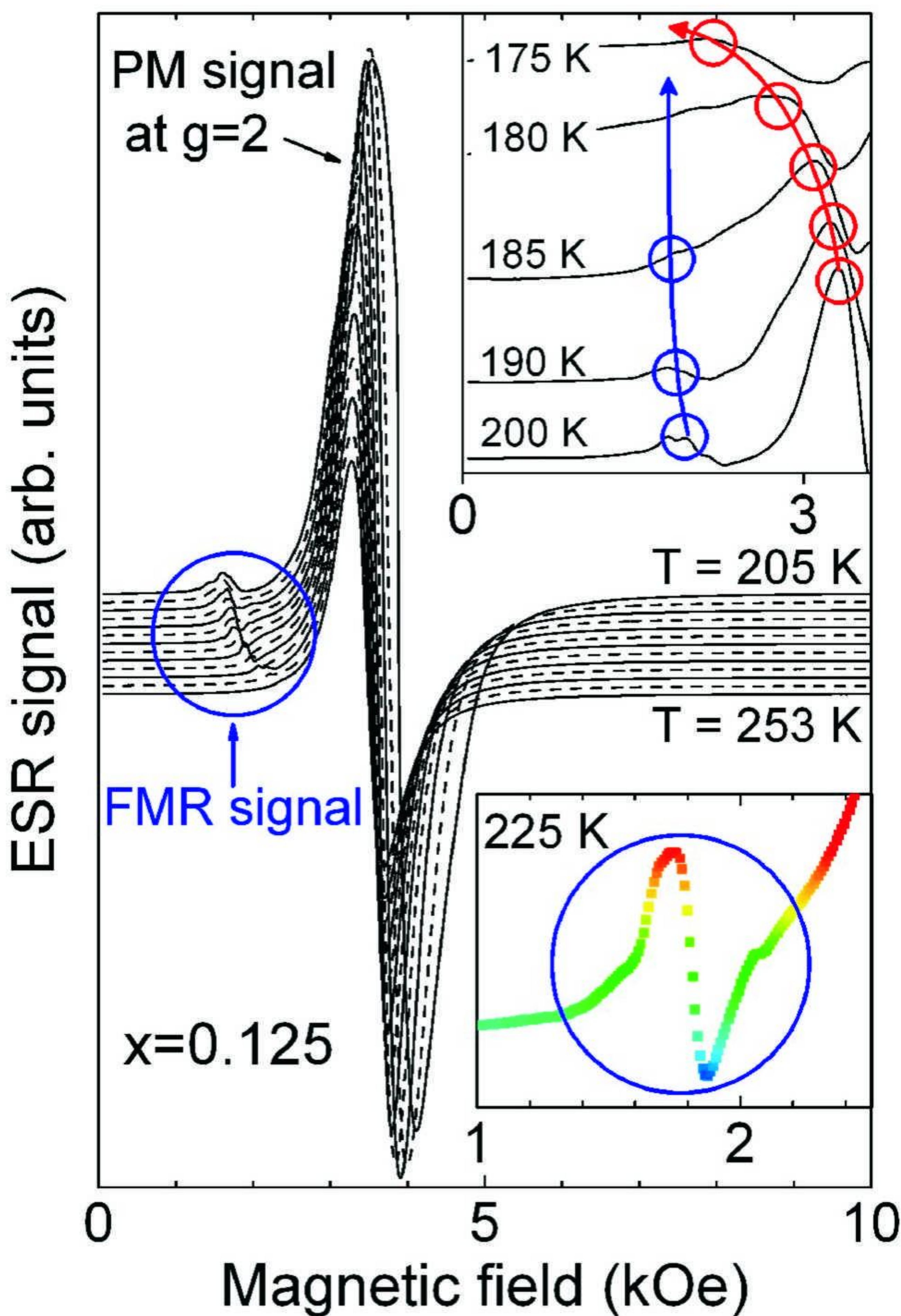
**Figure 3** 2D-Contour Plot of the ESR spectra vs  $T$  and  $H$  for  $x=0.125$ . The expanded plot clearly shows the emerging of the FMR from the PM signal with decreasing temperature. The plot was obtained by interpolation of 34 spectra.

**Figure 4** Comparison of magnetic susceptibility and ESR. Temperature dependence of **a**, the ac susceptibility ( $H_{ac}=1$  Oe,  $f_{ac}=9.999$  Hz) and the inverse magnetic susceptibility at 10 Oe and 1 kOe, and **b**, the resonance fields of the FMR and the PM signal for  $x = 0.1$ . The solid line describes the FMR shift  $\sim(1-T/T_G)^{1/2}$ . The PM signal shifts to lower fields due to the strong increase of the susceptibility on approaching magnetic order (compare upper inset in Fig. 2). The external magnetic field was applied within the easy plane. Error bars correspond to the linewidth of the FMR and the PM signal, respectively.

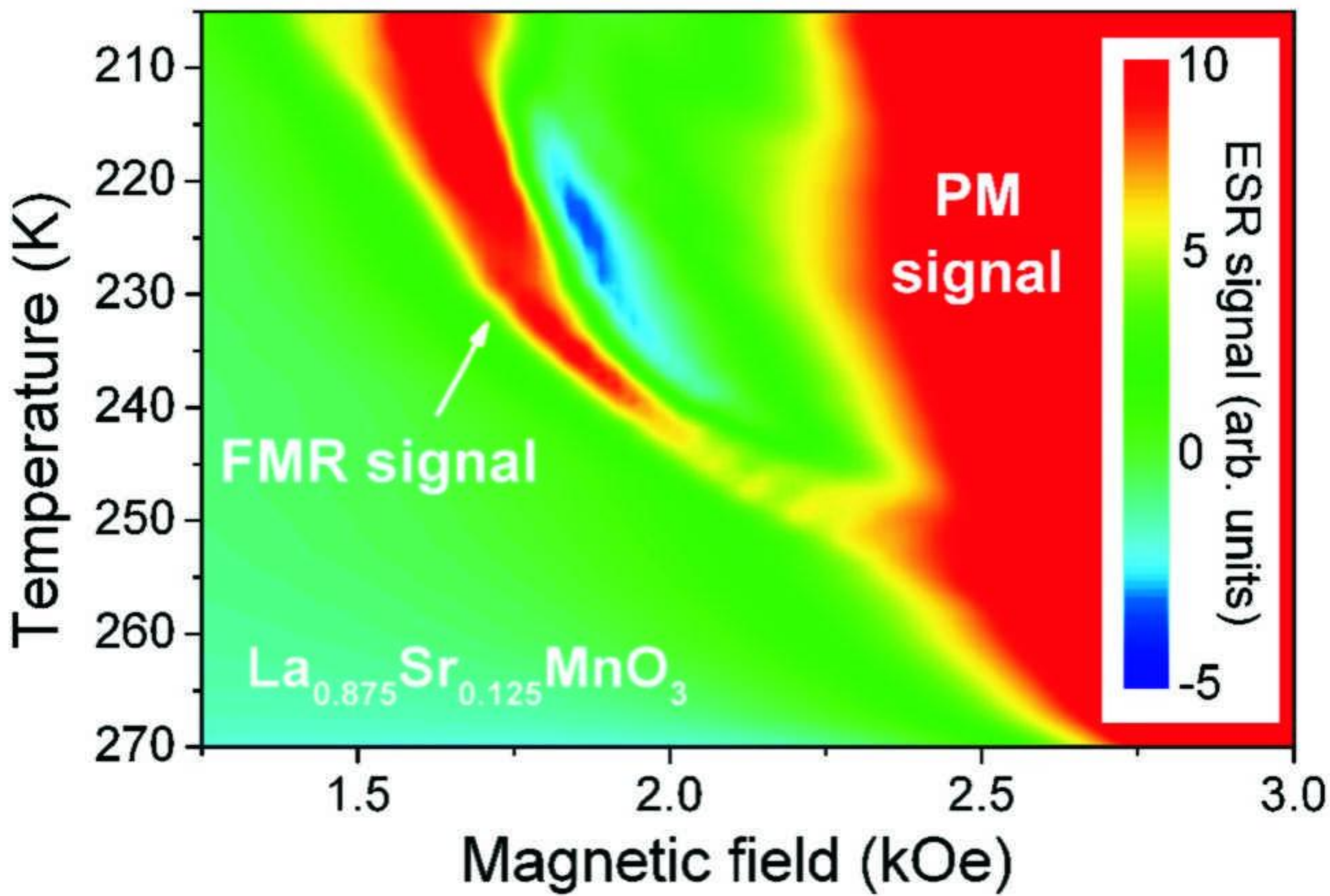
# Deisenhofer\_Fig1



# Deisenhofer Fig2



# Deisenhofer\_Fig3



# Deisenhofer\_Fig4

